# Chemical creep and its effect on contact ageing

*Zhuohan Li and Izabela Szlufarska*

Department of Materials Science and Engineering, University of Wisconsin-Madison, Madison, 53706-1595, USA

**Abstract**

Materials age and their properties can evolve over time scales that in many cases can be captured in laboratory experiments. Creep is one of the most commonly observed ageing phenomena, and the underlying mechanisms typically involve continuous plastic deformation or diffusion under the applied stress. In the elastic regime and at room temperature, time-dependent deformation is not expected in typical solids, unless the material is viscoelastic. Here, we performed multi-scale simulations and discovered that deformation creep, and thus, time evolution of the contact area can occur at interfaces between solid materials in the absence of plasticity, diffusion, or viscoelasticity. This creep takes place when material interface is reactive, and it arises from the successive formation of adhesive interfacial chemical bonds that pull the surfaces towards each other. Those chemical bonds not only increase the contact area, but also enhance the shear strength, resulting in a synergic effect on ageing of frictional contacts, where the static friction increases with the contact time. Our work provides a new contact creep mechanism, and furthermore, reveals that contact ageing can originate from not just the increase in the "contact quantity" — contact area, but also from the "contact quality" — shear strength, and more importantly, the two mechanisms are not necessarily independent of each other.

Under a constant applied load materials can undergo creep, and the underlying time-dependent deformation mechanisms include atomic diffusion[1,2], dislocation motion[3], and molecular chain rearrangement[4]. Creep is also relevant for interfaces under mechanical loads. The local contact pressure can vary significantly across the interface due to the surface roughness[5], which can result in asperity creep where the local pressure is high enough to cause permanent plastic deformation. Indeed, the increase in the contact area due to plastic deformation and creep has been reported experimentally[6,7].

Quantification of the contact area has been pursued since the pioneering work by Hertz in 1882[8], which is of practical importance, as the contact area affects various physical properties at the material interface, such as friction, heat transfer, and electronic conductivity. Specifically, the contact area, $A$, is related to the friction force $F$ through the equation $F = \tau \times A$, where $\tau$ is the interfacial shear strength. Thus, an increase in the contact area due to the asperity creep will result in increase in the static friction — a phenomenon called contact ageing.

Contact ageing exists in a wide range of materials [9–12] and is believed to play critical roles in multiple fields and applications, including earthquake mechanics[13], wafer bonding[14], and nano/micro-electromechanical systems[15]. The aging mechanism by asperity creep is often referred to as the "contact quantity" hypothesis, as it is related to the change in the number of physical contacts across the interface.[6,11,16,17]. The "contact quality" hypothesis is another major hypothesis, where the increase in friction $F$ is attributed to the time-dependent increase in the shear strength $\tau$,

and the contact area is instead assumed be a constant. The underlying physics of the "contact quality" hypothesis vary with materials, but is related to the time evolutions of the local physical and chemical state, such as better-pinned state of local atomic contacts[18], molecular densification[19], or interfacial chemical bonding[10,20–22].

Up to now, the two contact ageing hypotheses have been investigated mostly independently, assuming one of them, i.e., increase in the area $A$ or shear strength $\tau$, is the major or the only reason for the increase in the static friction $F$. Only a few recent papers reporting scenarios where both the quantity and the quality of contact contribute to contact aging at the same time[18,19]. In the study reported in Ref. [18], which was carried out on a silicon-graphene interface, the true contact area increases due to the puckering of the graphene (quantity increase), and the shear strength increases because local atomic contacts evolve towards a more commensurate and better-pinned state (quality increase). In Ref. [19], the increase in friction at an interface between two polymers has been attributed to a combination of the creep flow of the asperity (quantity increase) and the local densification of molecules, which in turn inhibits intermolecular twists (quality increase). In both cases, although the increases in contact quality and contact quantity occur simultaneously, these two effects are not coupled to each other and have fundamentally different underlying physical mechanisms.

Here, we use molecular dynamics (MD) and kinetic Monte Carlo (kMC) simulations to demonstrate a new mechanism for the asperity contact creep and consequently for the contact aging, termed chemical creep. We discovered that the contact area can evolve over time, even for the pure elastic contact, as a result of the successive formation of adhesive chemical bonds across the interface, such as siloxane bonds at $SiO_2$-$SiO_2$ interfaces[23], which pull the contacting surfaces towards each other, leading to an increase in the contact area of asperities. At the same time, these interfacial bonds will also increase the resistance to the horizontal frictional shearing, as previously proposed as the chemical origin of "contact quality" hypothesis[10,20–22]. In other words, the mechanical strength of interfaces, e.g., the static friction, can be simultaneously increased by the change in both the contact area (quantity) and the shear strength (quality) by means of the same underlying process – interfacial chemical bonding.

The chemical creep occurs due to the finite additional normal force that arises from the formation of chemical bonds across the interface. Here, we define the normal force induced by the formation of an interfacial chemical bond as bond-induced force. In order to sample physically realistic distribution of the bond-induced forces, we use amorphous silica-silica interfaces as an example. Specifically, we prepared two slabs of amorphous silica with hydroxylated surfaces, and we put the two slabs into contact as shown in Fig. 1. Siloxane bonds at different interfacial positions are formed by hand for those Si-Si pairs that are within the cut-off distance of 3.6 Å[24]. Those interfacial Si-Si pairs that are already bridged by O (defined based on the Si-O cutoff distance of 1.8 Å[24]) in the initial configuration when the upper and the lower slabs are brought into the contact are not included for sampling the bond-induced force.

The indentation depth of slab-slab contacts (both bonded and unbonded interfaces) is changed successively by moving the upper slab towards or against the lower slab with a step of at most 0.04 Å, and the contact pressure is calculated at each indentation depth. The contact pressure is calculated by dividing the time-averaged normal force applied to the fixed boundary layers, as shown in Fig. 1 (a), by the nominal area of the interface. Here, the 0 Å indentation depth is defined as the depth at which the slabs are initially brought into contacts at which the bonds are formed manually. The range of indentation depths that we chose is from -1.2 Å (the lowest contact pressure) to 1.2 Å (the highest contact pressure), which corresponds to the contact pressures of a unbonded

interface from 0.9 to 6.9 GPa. We repeat this process for 4 different interfaces. Here, the different interfaces are created by moving the upper slab horizontally within the plane of the interface. We identified two types of bonding mechanisms: mechanism 1 (condensation): $Si_{up}$-OH + $Si_{low}$-OH = $Si_{up}$-O-$Si_{low}$ + $H_2O$, and 2) and mechanism 2 (swapping): $Si_{up}$-OH + $Si_{low}$-O-$Si_{low}$ = $Si_{up}$-O-$Si_{low}$ + $Si_{low}$-OH. In this notation, $Si_{up}$ and $Si_{low}$ are silicon atoms in the upper and lower silica slabs, respectively. From the 4 interfaces, 13 instances of mechanism 1 and 4 instances of mechanism 2, indicating mechanism 1 is about 3 times more likely than mechanism 2 for an amorphous silica-silica interface.

In Fig. 1 (b), we show the calculated bond-induced force as a function of the indentation depth for both bonding mechanisms 1 and 2, where the negative (positive) value means the bond is adhesive (repulsive). We calculate the change in the contact load upon forming one single bond at fixed indentation depth, and the bond-induced force is averaged across all the interfaces. As it can be seen, both bonding mechanisms are adhesive, i.e., -0.56 nN and -0.37 nN on average for mechanism 1 and 2, respectively, and the bonds formed by mechanism 1 are slightly more adhesive than by mechanism 2. With the error bars taken into consideration, the range of bond-induced forces for the silica-silica interface falls approximately in the range from – 1.0 to 0.4 nN. We also conducted additional MD simulations to check whether pre-existing interfacial bonds on nearby sites affect the bond-induced force (see S3 in Supporting Information). Our simulation results indicate that the effect from the neighboring bonds is limited, where the bond-induced force only differs by ~ 0.1 nN from the one calculated without neighboring bonds. The specific value of the bond-induced force may also depend on the environment (e.g., pH, humidity, etc). However, it is not our goal to provide a quantitative value of bond-induced force for any surface, but instead to demonstrate that the order of magnitude of the bond-induced force is large enough to induce chemical creep.

Our simulations also show that for mechanism 1, there is a slightly increasing trend of bond-induced force (i.e., bonds become less adhesive) as the indentation depth is increased. This could be understood that as the slab is indented more, the reaction site becomes more repulsive. Conversely, when the contacting surfaces move away from each other, the bond is stretched and becomes more adhesive/attractive. In contrast to mechanism 1, for mechanism 2 there is no clear monotonic trend in the bond-induced pressure vs. indentation depth. Such difference can originate from the bonding energetics or the strain energy stored in the surrounding bulk[23], but the exact physical origin is unclear. Nonetheless, our current simulation results clearly demonstrate that the chemical bonding at the material interfaces indeed induces a change in the normal force in the contacts.

When experiments are carried out at a constant load, as often set as the boundary condition in atomic force microscopy (AFM)[10,21,25], formation of interfacial chemical bonds with non-zero bond-induced force will lead to a change in the separation distance between the sliding tip and the substrate in order to compensate for the change in the normal load. The change in the surface separation will in turn result in a change in the asperity indentation depth and the contact area, i.e., chemical creep, following whichever load-area relationship is appropriate for a given contact mechanics[26]. In order to further demonstrate that such bond-induced force also exists in the round tip – flat substrate contacts, we also conducted MD simulations to calculate the bond-induced force at tip-substrate contact with the tip radius of 9 nm, where the system size is large enough to show that the strain is localized near the interface (see section S4 in the Supporting Information for computational details). The average bond-induced forces at the tip-substrate contact obtained for mechanisms 1 and 2 are -0.31 nN and -0.36 nN, respectively, which both is on the same order of

magnitude of the average bond-induced force obtained for the flat slab-slab contacts, as shown in Fig. 1 (b). The negative value obtained for the large tip-substrate contact further indicate the adhesive nature of the interfacial siloxane bonds. Our MD simulations on tip-substrate contact also show that the contact area has increasing trend with the normal load, as expected from the conventional single asperity contact mechanics models (see Fig. S3 in Supporting Information). Therefore, our simulation results indicate that the chemical creep can indeed occur for tip-substrate contacts, which is due to the interfacial adhesive bonds that increases the normal load.

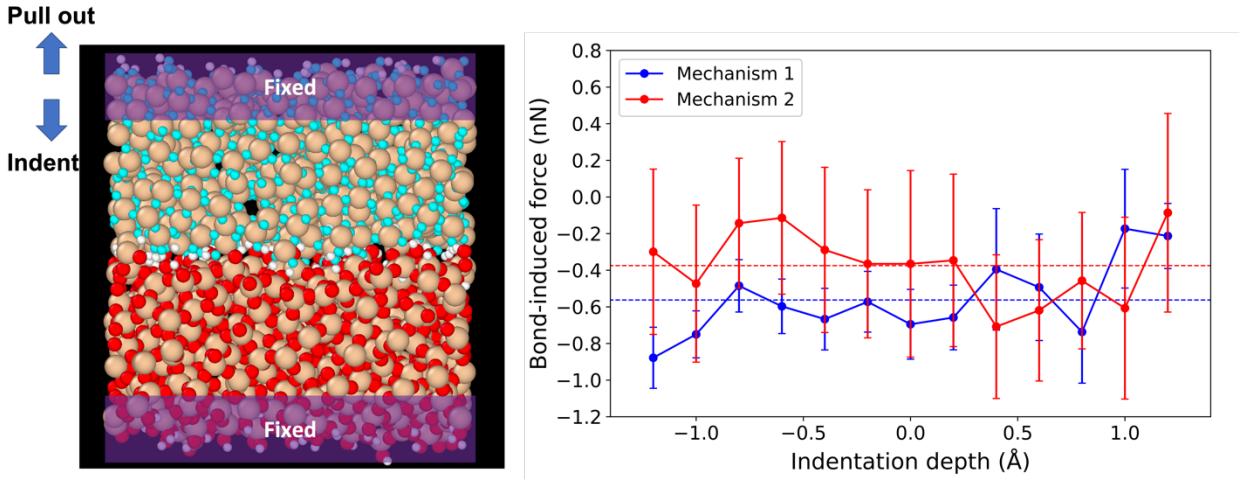


*Figure 1 (a) Contacting amorphous silica slabs used in MD simulations. The top and bottom 7 Å layers are fixed during the simulations. The indentation depth is changed by successively moving the upper slab in the vertical direction. The red, cyan, beige, and white colors represent, O in the lower slab, O in the upper slab, Si, and H, respectively.* (b) *Bond-induced force as a function of the indentation depth for different bonding mechanisms calculated using classical MD simulations. Blue and red data is sampled from the bonded interface with reaction mechanisms 1 and 2, respectively. The error bars are standard error of the mean of bond-induced forces at a given indentation depth, and the dashed horizontal lines are the mean values averaged over different indentation depths.*

In order to estimate how a bond-induced force affects the contact area, and how it further affects the contact ageing, we adapted the kMC model originally developed for simulating the formation of bonds within a fixed nominal contact area of single asperity contacts[20,27]. In our original kMC model[27], the nominal contact area is pre-determined by the Derjaguin, Muller, and Toporov (DMT) contact model[28] with a given normal load and a pull-off adhesion force. The number of reaction sites is then calculated assuming a surface density of Si-OH group[2 29]. The schematic visualization of the original kMC model is shown in Figs. 2 (a) and (b), where the white color represents surface sites outside the contact region (not available for bonding), and blue and pink, respectively, represent unbonded and bonded sites within the contact region. In the case of silica-silica interface, the white and blue sites represent out-of-contact and in-contact silanol groups (Si-OH), respectively, and the pink site represents the siloxane bond (Si-O-Si). Before the simulation starts, all the reaction sites are initially set to the unbonded state, as shown in Fig. 2 (a), where the energy barrier for chemical reaction at each site is sampled from a given distributions. As the simulation evolves, bonds form at reaction sites that are randomly selected based on the

probabilities determined by the energy barriers. The counts of pink sites at the end of the simulation, as shown in Fig. 2 (b), represents the number of interfacial bonds.

Here, the kMC model has been further developed to enable a change of the nominal contact area throughout the simulation by updating the total normal load every time a new bond is formed. If the nominal contact area is increased by forming adhesive bonds, which is calculated using the DMT model with the updated adhesive force, the corresponding number of new unbonded sites are selected randomly and added in the periphery of the original contact region. On the other hand, if the nominal contact area is reduced by forming repulsive bonds, the unbonded reaction sites at the periphery of the contact are removed from kMC simulations. Fig. 2 (c) show the schematic visualization of the kMC simulation that allows for an increasing in the nominal contact area. In our new kMC model, we also assume that the increase in the static friction measured at the end of the ageing is proportional to the number of interfacial bonds, which has been justified previously[30]. No plastic deformation is explicitly included, as the main goal is to investigate the coupling of the chemical bonding and the chemical creep in the elastic regime. Indeed, the range of contact pressures we obtained from our MD simulations is about 1-7 GPa, which are below the experimentally determined indentation hardness of amorphous silica of ~10 GPa[31].

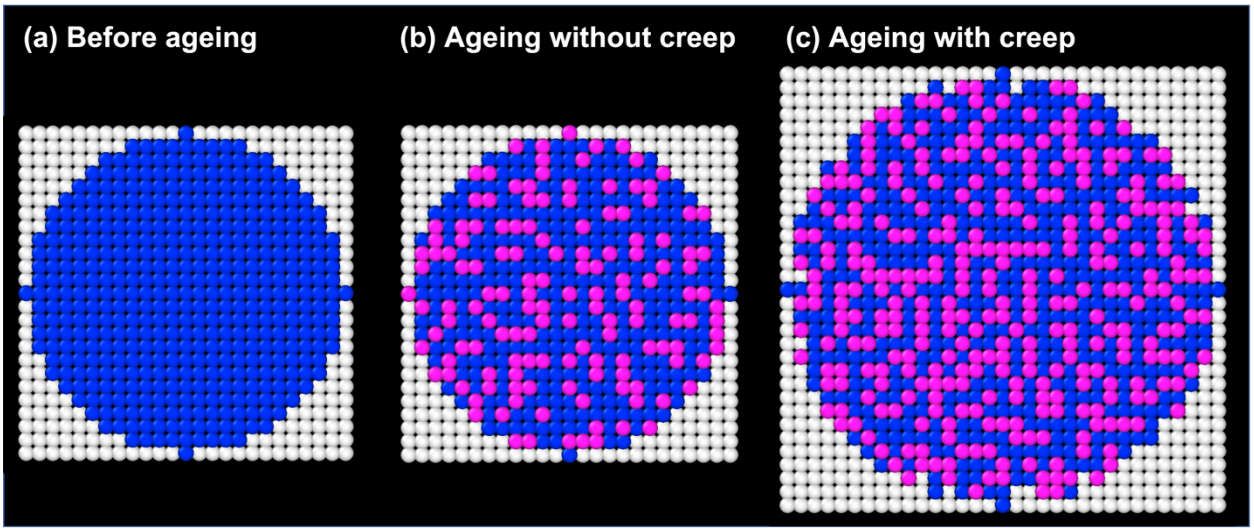


*Figure 2 Schematic picture of the kMC simulation. (a) Before, (b) during the simulation without any creep and (c) during the simulation with creep. Blue and pink are unbonded sites (e.g., Si-OH) and bonded sites (e.g., Si-O-Si) within the contact, respectively. White represents sites (e.g., Si-OH) that are outside of the contact region. The size of each rection site is determined by the surface density of silanol groups*[29].

In principle, in order to simulate real material interfaces, the energy barriers at each reaction site with different local atomic configurations should be known *a priori*. Such approach would require a large number of quantum mechanical calculations. Here, instead of simulating amorphous silica-silica interfaces with specific atomic configurations, we examine two general interfacial scenarios with different energy barrier distributions, i.e., 1) exothermic interface and 2) endothermic interface, as shown in Fig. 3 (a). The ranges for energy barriers, $E_{b,form}$, for bond formation were chosen to fall in a physically-justifiable range based on previous theoretical studies of silica-silica interfaces [20,27,32]. The range of energy barriers for bond breaking, $E_{b,form}$, is shifted

from that of $E_{b,form}$ in the opposite directions for the two scenarios, which creates different numbers of exothermic and endothermic reaction sites across the interface. The exothermic and the endothermic interface can each have negative (exothermic) and positive (endothermic) reaction energy sites, but the former interface has a greater number of negative reaction energy sites than the positive ones and vice versa. The qualitative trend obtained from our kMC simulations should be universal for other material interfaces with similar chemical bonding energetics.

For the specific case of silica-silica interface considered earlier, we obtained the reaction energy for bond formation as a function of the indentation depth (see Fig. S5 Supporting Information). Our results show that the reactions sampled in our silica-silica interfaces are exothermic on average. Previous ReaxFF MD simulation showed that there can also be endothermic reactions at the amorphous silica-silica interface[20]. Our previous work based on *ab initio* calculations at the crystalline $SiO_2$-$SiO_2$ interfaces also showed that the bonding reaction can be endothermic[23]. Fully determining the reaction energetics of all the possible reactions at the amorphous silica-silica interface are computationally expensive, which is left for future study.

We also assume that the bond-induced force, $F_{bond}$, of different reaction sites follows a Gaussian distribution, under the assumption that the amorphous surface has random local atomic configurations that lead to the variation in the bond-induced force. In the following, kMC simulations are performed with two different distributions, where the mean value of the distribution $\langle F_{bond} \rangle$ is set either to - 0.4 nN or - 0.2 nN, as shown in Fig. 3 (b). The range of the distributions of $F_{bond}$ agrees with the range obtained by our MD simulations (Fig. 1 (b)). The interface simulated with distribution around $\langle F_{bond} \rangle$ = - 0.4 nN contains bonds that are overall more adhesive compared to the interface with $\langle F_{bond} \rangle$ = - 0.2 nN. In both cases, we assume that the distribution of bond-induced force does not change during the ageing, even if the asperity is indented more due to the chemical creep. Other parameters used in the kMC simulations are listed in Supporting Information, which are set according to the typical AFM experimental setups for single asperity contact ageing measurements, and consistently with our earlier kMC models that were fitted to AFM experiments of contact ageing on amorphous silica-silica interfaces.

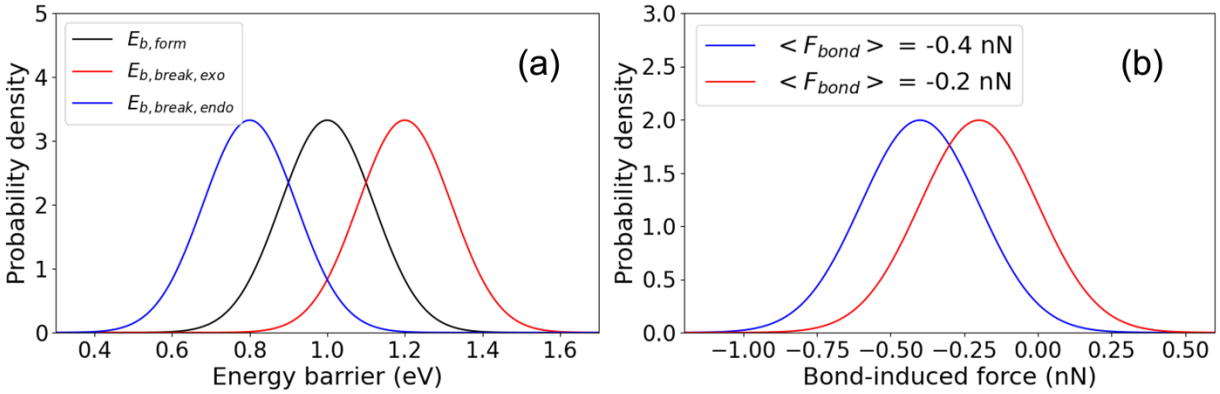


*Figure 3 (a) Energy barrier distributions. The black curve is the energy barrier for bond formation, $E_{b,form}$. The red and the blue curves are the energy barrier for bond breaking, $E_{b,break}$ for exothermic and endothermic interfaces, respectively. (b) The two different distributions of bond-induced force, $F_{bond}$, used in the kMC simulations. $\langle ... \rangle$ in the legend represents the mean of the distribution.*

Figures 4 (a) and (b) show simulation results for the exothermic interface for different values of $\langle F_{bond} \rangle$, where the number of interfacial bonds and of the nominal contact area evolves with

time. The logarithmic increase in the number of bonds (and therefore also the static friction) with time is observed for all cases, and it extends to times larger than $10^5$ s. Interestingly, the nominal contact area also increases logarithmically with non-zero bond-induced force. Similar logarithmic increase in the contact area was previously observed experimentally for different types of material interfaces, including soda-lime float glass[6], acrylic plastic[6] and the quartz interfaces[7], where the mechanisms for the contact creep were not clear. Our simulation results indicate that for those interfaces where interfacial chemical bonding is possible, the chemical bonding should be taken into the consideration as an important factor for the contact creep, especially in the elastic contact regime. In the case where sever plastic deformation occurs at higher contact pressures, it is possible that both the plastic creep and the chemical creep contribute to the increase in the contact area.

The increase in the contact area and in the number of bonds form a positive feedback loop. The increase in the nominal contact area provides more available reactions sites for chemical bonding. This in turn will result in more adhesive interfaces, and therefore a larger contact area. As a result, the rate of contact ageing is faster for an interface that forms adhesive bonds ($F_{bond} < 0$) than an interface whose bond is non-adhesive ($F_{bond} = 0$). It can be seen from Fig. 4 (a) that the effect of chemical creep on contact ageing becomes more significant if the bond is more adhesive (more negative $F_{bond}$).

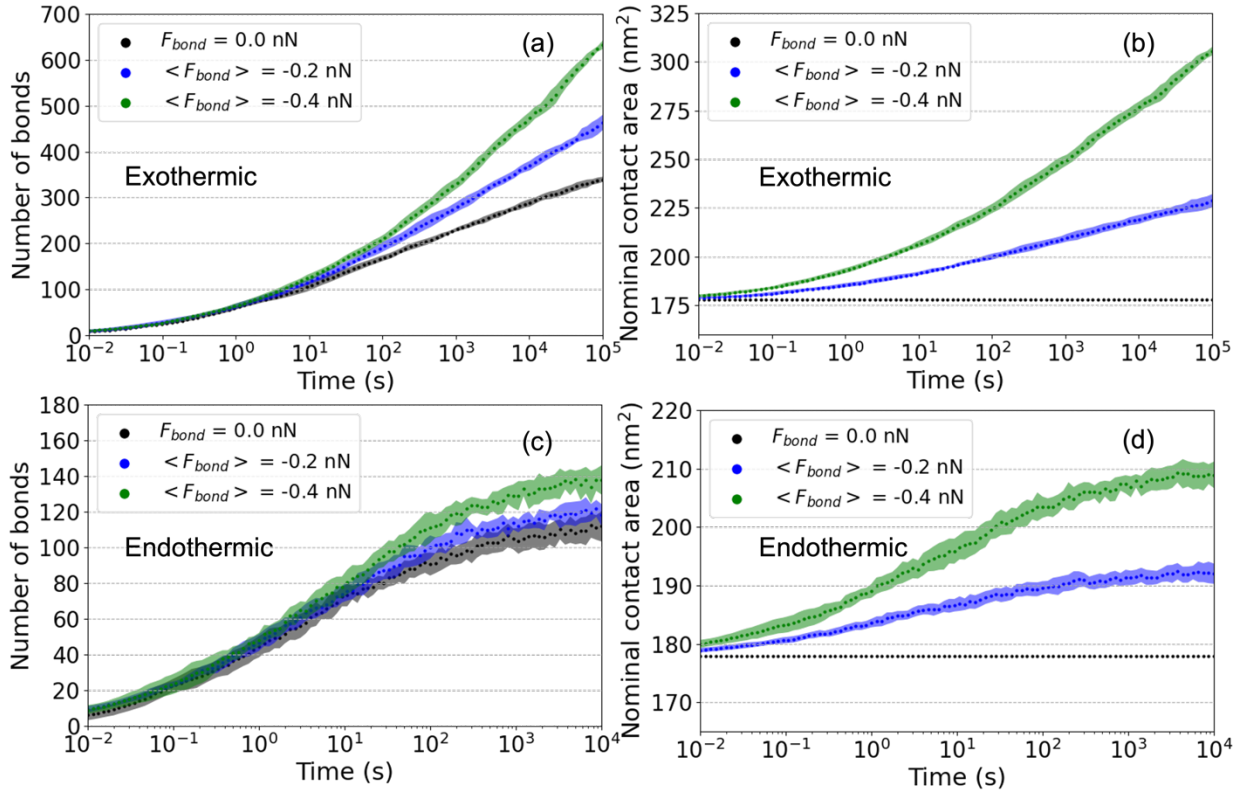


*Figure 4 Results of kMC simulations of time evolution of the number of bonds and the nominal contact area for [(a) and (b)] exothermic interface, and [(c) and (d)] endothermic interface with different distributions of bond-induced force $F_{bond}$. All data points represent values averaged over 10 simulations with different random seeds and the shaded area corresponds to the standard deviation from the average.*

Next, we perform kMC simulations on the endothermic interface, where the number of sites energetically unfavorable for bonding is larger than the number of sites that are energetically favorable. The results are shown in Figs. 4 (c) and (d). Fig. 4 (c) reveals that the dependence of the number of bonds (and therefore also the static friction) on time is still logarithmic, similarly to what the model predicts for the exothermic interface. However, here the saturation of the logarithmic dependence occurs for times larger than $10^2$ s. Interestingly, the nominal contact area also shows similar logarithmic and saturation behaviors with respect to the number of bonds, as shown in Fig. 4 (d).

It is clear that for an endothermic interface, the effect of chemical creep is much smaller than in the case of exothermic interface. This is because the chemical creep can only be manifested when there are sufficient number of bonds formed across the interface. The bonding event is thermodynamically less likely for an endothermic interface, and therefore one can expect a much smaller increase in the nominal contact area. Nonetheless, the fact that the contact area still increases for endothermic interfaces, as long as the interfacial bond is adhesive on the average, indicates that the chemical creep can possibly occur on a wide range of material interfaces, and affect other material properties that depend on the interfacial contact area, such as heat transfer and electronic conductivity.

The fact that in the presence of chemical creep, the number of bonds increases logarithmically with time is also of significance. In previous studies on silica-silica interfaces[10,20,25,27], the logarithmic time dependence of the number of bonds, and therefore the static friction, was considered to originate purely from the heterogeneity of the kinetics of chemical reaction, where the reaction rates of chemical bonding vary among the reaction sites across the interface, under the assumption of a fixed contact area throughout the ageing. Here, our results demonstrate that contact area can also increase as a result of the same chemical process, even in the elastic regime, and such coupling between chemical reactions and the contact creep does not change the qualitative trend of logarithmic time dependence on the number of interfacial bonds. The previous assumption on the fixed contact area may still be effective, considering that in our simulations, the increase in the number of bonds due to the chemical creep is only significant for $> 10^2$ s even for the exothermic interface, as shown in Figs. 4 (a) and (c), while the AFM experiments only measure the contact ageing up to $10^2$ s[10,25]. Our simulation results call for careful experimental characterization of the contact area evolution during ageing, especially for the long time contact ($> 10^2$ s), where the interfacial chemical bonding is considered to be the major contributions for the logarithmic time dependent static friction. Understanding the contact ageing behavior at longer contact times is important for understanding the earthquake nucleation and recurrence[13]. Ignoring the evolution of contact area in those contact ageing experiments might cause overestimation of the interfacial chemical bonding kinetics (lower energy barriers to bond formation), higher surface density of reaction sites, or higher bond rupture force upon shearing than it should be.

Our work demonstrates that the interfacial chemical bonding in the so-called static contacts will cause quite dynamic evolution of both the chemical and the mechanical states of the material interfaces. It shows that “contact quantity” and “contact quality” are not necessarily distinct from each other as they can be governed by the same underlying mechanism. For future studies, it will also be highly valuable to investigate the significance of such chemical creep on rough contacts at larger length scales, both theoretically and experimentally, where even more physical and chemical phenomena could be coupled to each other across different length-scales, including the elastic and the plastic deformation, the interfacial chemical reactions, the chemical creep, and even the conventional mechanical plastic creep.

**Acknowledgment**

The authors gratefully acknowledge financial support from the National Science Foundation, Grant No. 1951314, fruitful discussions with R. Carpick, D. Goldsby, and J. B. McClimon from the University of Pennsylvania, and James Batteas, George M. Pharr, and Abhijeet Gujrati from Texas A&M University.

**Supporting Information**

- Computational methods
- Water-induced force and the potential energy of interfacial water molecule
- Bond-induced force from multi-bond interfaces
- Tip-substrate contacts and the contact mechanics
- Reaction energy of interfacial siloxane bonding
- Mechanochemical effect in chemical creep

**References**

(1) F. R. N. Nabarro. Report of a Conference on the Strength of Solids. In *Physical Society, London*; 1948; p 75.
(2) Coble, R. L. A Model for Boundary Diffusion Controlled Creep in Polycrystalline Materials. *J. Appl. Phys.* **1963**, *34*, 1679–1682. https://doi.org/10.1063/1.1702656.
(3) PM, A.; JP, H.; J., L. *Theory of Dislocations*; Cambridge University Press: Cambridge, UK, 2017.
(4) I. M. Ward, J. S. *Mechanical Properties of Solid Polymers: Third Edition*; John Wiley and Sons Ltd, 2012.
(5) Persson, B. N. J.; Albohr, O.; Tartaglino, U.; Volokitin, a I.; Tosatti, E. On the Nature of Surface Roughness with Application to Contact Mechanics, Sealing, Rubber Friction and Adhesion. *J. Phys. Condens. Matter* **2005**, *17*, R1–R62. https://doi.org/10.1088/0953-8984/17/1/R01.
(6) Dieterich, J. H.; Kilgore, B. D. Direct Observation of Frictional Contacts: New Insights for State-Dependent Properties. *Pure Appl. Geophys. PAGEOPH* **1994**, *143*, 283–302. https://doi.org/10.1007/BF00874332.
(7) Goldsby, D. L.; Rar, A.; Pharr, G. M.; Tullis, T. E. Nanoindentation Creep of Quartz, with Implications for Rate-and State-Variable Friction Laws Relevant to Earthquake Mechanics. Journal of Materials Research. *J. Mater. Res.* **2004**, *19*, 357–365. https://doi.org/10.1016/0040-1951(83)90266-4.
(8) Hertz, H. Ueber Die Berührung Fester Elastischer Körper. *J. für die reine und Angew. Math.* **1882**, *92*, 156–171.
(9) Carpenter, B. M.; Ikari, M. J.; Marone, C. Laboratory Observations of Time-Dependent Frictional Strengthening and Stress Relaxation in Natural and Synthetic Fault Gouges. *J. Geophys. Res. Solid Earth* **2016**, *121*, 1183–1201. https://doi.org/10.1002/2015JB012136.
(10) Li, Q.; Tullis, T. E.; Goldsby, D.; Carpick, R. W. Frictional Ageing from Interfacial

Bonding and the Origins of Rate and State Friction. *Nature* **2011**, *480*, 233–236. https://doi.org/10.1038/nature10589.
(11) Mazo, J. J.; Dietzel, D.; Schirmeisen, A.; Vilhena, J. G.; Gnecco, E. Time Strengthening of Crystal Nanocontacts. *Phys. Rev. Lett.* **2017**, *118*, 246101. https://doi.org/10.1103/PhysRevLett.118.246101.
(12) Feldmann, M.; Dietzel, D.; Fuchs, H.; Schirmeisen, A. Influence of Contact Aging on Nanoparticle Friction Kinetics. *Phys. Rev. Lett.* **2014**, *112*, 155503. https://doi.org/10.1103/PhysRevLett.112.155503.
(13) Marone, C. Laboratory-Derived Friction Laws and Their Application To Seismic Faulting. *Annu. Rev. Earth Planet. Sci.* **1998**, *26*, 643–696. https://doi.org/10.1146/annurev.earth.26.1.643.
(14) Plößl, A.; Kräuter, G. Wafer Direct Bonding: Tailoring Adhesion between Brittle Materials. *Mater. Sci. Eng. R Reports* **1999**, *25*, 1–88. https://doi.org/10.1016/S0927-796X(98)00017-5.
(15) Corwin, A. D.; de Boer, M. P. Frictional Aging and Sliding Bifurcation in Monolayer-Coated Micromachines. *J. Microelectromechanical Syst.* **2009**, *18*, 250–262. https://doi.org/10.1109/JMEMS.2008.2011717.
(16) Ikari, M. J.; Carpenter, B. M.; Marone, C. A Microphysical Interpretation of Rate- and State-Dependent Friction for Fault Gouge. *Geochemistry, Geophys. Geosystems* **2016**, *17*, 1660–1677. https://doi.org/10.1002/2016GC006286.
(17) Dillavou, S.; Rubinstein, S. M. Nonmonotonic Aging and Memory in a Frictional Interface. *Phys. Rev. Lett.* **2017**, *120*, 224101. https://doi.org/10.1103/PhysRevLett.120.224101.
(18) Li, S.; Li, Q.; Carpick, R. W.; Gumbsch, P.; Liu, X. Z.; Ding, X.; Sun, J.; Li, J. The Evolving Quality of Frictional Contact with Graphene. *Nature* **2016**, *539*, 541–546. https://doi.org/10.1038/nature20135.
(19) Petrova, D.; Sharma, D. K.; Vacha, M.; Bonn, D.; Brouwer, A. M.; Weber, B. Ageing of Polymer Frictional Interfaces: The Role of Quantity and Quality of Contact. *ACS Appl. Mater. Interfaces* **2020**, *12*, 9890–9895. https://doi.org/10.1021/acsami.9b19125.
(20) Liu, Y.; Szlufarska, I. Chemical Origins of Frictional Aging. *Phys. Rev. Lett.* **2012**, *109*, 186102. https://doi.org/10.1103/PhysRevLett.109.186102.
(21) Vorholzer, M.; Vilhena, J. G.; Perez, R.; Gnecco, E.; Dietzel, D.; Schirmeisen, A. Temperature Activates Contact Aging in Silica Nanocontacts. *Phys. Rev. X* **2019**, *9*, 041045. https://doi.org/10.1103/PhysRevX.9.041045.
(22) Li, S.; Zhang, S.; Chen, Z.; Feng, X.; Li, Q. Length Scale Effect in Frictional Aging of Silica Contacts. *Phys. Rev. Lett.* **2020**, *125*, 215502. https://doi.org/10.1103/PhysRevLett.125.215502.
(23) Li, Z.; Szlufarska, I. Physical Origin of the Mechanochemical Coupling at Interfaces. *Phys. Rev. Lett.* **2021**, *126*, 76001. https://doi.org/10.1103/PhysRevLett.126.076001.
(24) Li, A.; Liu, Y.; Szlufarska, I. Effects of Interfacial Bonding on Friction and Wear at Silica/Silica Interfaces. *Tribol. Lett.* **2014**, *56*, 481–490. https://doi.org/10.1007/s11249-014-0425-x.
(25) Tian, K.; Gosvami, N. N.; Goldsby, D. L.; Liu, Y.; Szlufarska, I.; Carpick, R. W. Load and Time Dependence of Interfacial Chemical Bond-Induced Friction at the Nanoscale. *Phys. Rev. Lett.* **2017**, *118*, 076103. https://doi.org/10.1103/PhysRevLett.118.076103.
(26) Carpick, R. W.; Ogletree, D. F.; Salmeron, M. A General Equation for Fitting Contact

Area and Friction vs Load Measurements Robert. *J. Colloid Interface Sci.* **1999**, *211*, 395–400.
(27) Li, Z.; Szlufarska, I. Multiphysics Model of Chemical Aging in Frictional Contacts. *Phys. Rev. Mater.* **2018**, *2*, 063602. https://doi.org/10.1103/PhysRevMaterials.2.063602.
(28) Derjaguin, B. V; Muller, V. M.; Toporov, Y. P. Effect of Contact Deformations on the Adhesion of Particles. *J. Colloid Interface Sci.* **1975**, *53*, 314–326.
(29) Zhuravlev, L. T. The Surface Chemistry of Amorphous Silica. *Colloids Surfaces A Physicochem. Eng. Asp.* **2000**, *173*, 1–38. https://doi.org/10.1016/S0927-7757(00)00556-2.
(30) Mo, Y.; Turner, K. T.; Szlufarska, I. Friction Laws at the Nanoscale. *Nature* **2009**, *457*, 1116–1119. https://doi.org/10.1038/nature07748.
(31) Oliver, W. C.; Pharr, G. M. An Improved Technique for Determining Hardness and Elastic Modulus Using Load and Displacement Sensing Indentation Experiments. *J. Mater. Res.* **1992**, *7*, 1564–1583. https://doi.org/10.1557/JMR.1992.1564.
(32) Tian, K.; Li, Z.; Liu, Y.; Gosvami, N. N.; Goldsby, D. L.; Szlufarska, I.; Carpick, R. W. Linear Aging Behavior at Short Timescales in Nanoscale Contacts. *Phys. Rev. Lett.* **2020**, *124*, 026801.

**Table of contents**

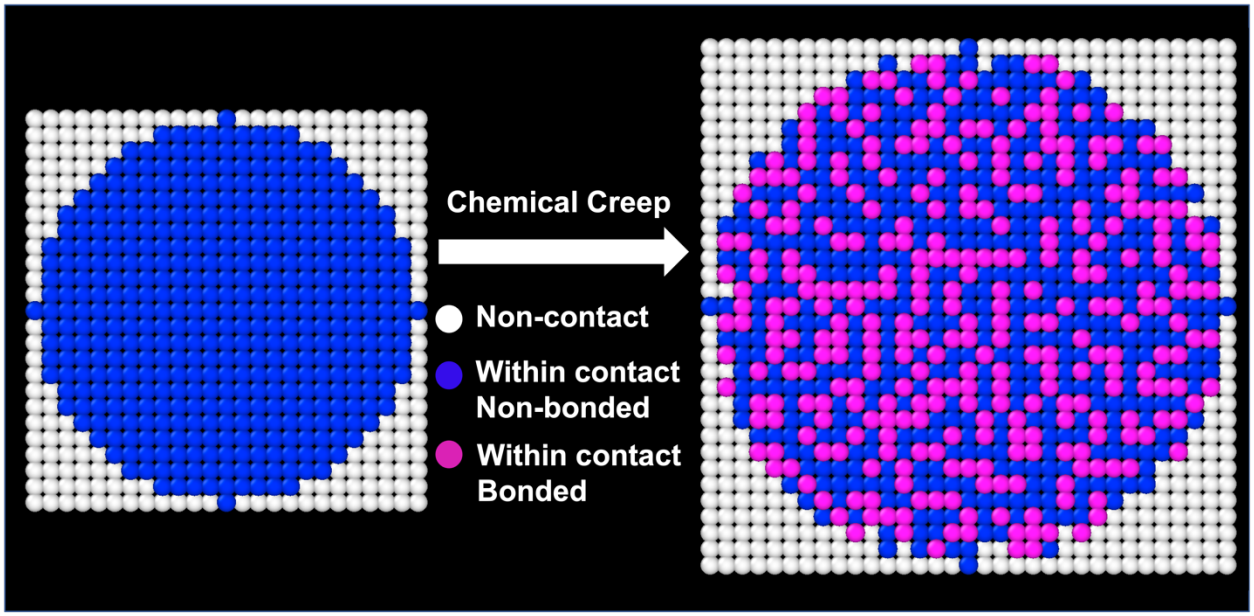

# Supporting Information to
# Chemical creep and its effect on contact ageing

*Zhuohan Li and Izabela Szlufarska*

Department of Materials Science and Engineering, University of Wisconsin-Madison, Madison, 53706-1595, USA

## S1. Computational Methods

We conducted MD simulations with ReaxFF reactive force field[1], which was optimized to capture the surface chemistry of hydroxylated amorphous silica. All MD simulations are performed with LAMMPS in NVT ensemble[2]. To create a flat amorphous silica slab, 3000-atom bulk silica model (1000 Si atoms and 2000 O atoms) with the density of 2.2 g/cm$^3$ [3] and periodic boundary conditions along all directions is first created through a melt and quench procedure, i.e., melted at 4000 K and quenched to 300 K with a quench rate of 5 K/ps. Then, a slab with the dimensions of 3.56 × 3.56 ×1.78 nm$^3$ is cut out from the bulk and periodic boundary conditions are removed from one of the directions to create two free surfaces. The slab is subsequently annealed at 1000 K for 200 ps. The free surfaces are then hydroxylated by including water molecules on each side of the slab, and then equilibrating the system at 300 K for 200 ps. We have also created a larger slab with the dimensions of 17.82 × 17.82 ×7.13 nm$^3$ by replicating the small substrate in all 3 spatial directions. A large spherical tip with the radius of 8.91 nm is cut out from the large slab, and both the large tip and the large slab are then annealed at 1050 K for 100 ps and quenched to 300 K with a quench rate of 10 K/ps. Both the tip and the slab are then hydroxylated by placing it inside a simulation box with bulk water, and then running simulations at 300 K for 200 ps. All the visualization of atomic system of MD simulations are done with OVITO[4].

The kMC model used in this study is built on our previous model[5]. The Eyring pressure effect on the energy barriers[6] and the elastic interactions on the energy barriers between the neighboring reaction sites[7] are included. Details on implementation of these effects can be found in references[5,7]. The parameters in the current kMC simulations are chosen to mimic previous AFM experiments. Specifically, the tip radius $R$ is 100 nm, the effective Young's modulus $E^*$ = 35.3 GPa[8], the total normal load (which is the sum of the applied load and the pull-off adhesion force) $L_{total}$ = 200 nN, temperature $T$ = 300 K, and the surface density of silanol group $\sigma_{OH}$ = 4 /nm$^2$ [9]. The attempt frequency for bond formation and breaking is $w = 10^{13}$ Hz, which is the typical atomic vibrational frequency. Other parameters are the same as used in the previous work[5] used to fit to the single asperity contact ageing experiments on silica-silica interfaces, except that here we assume that the bond rupture force across the interface is a constant during the course of ageing.

## S2. Water-induced force and the potential energy of interfacial water molecule

In the main text, we considered two types of reactions (mechanism 1 and 2). The condensation reactions (mechanism 1) will leave one water molecule at the interface, whereas there is no water molecule produced in the swapping mechanism (mechanism 2). For mechanism 1, the water molecule that should be produced at the interface by the bonding reaction is removed before the

indentation simulation. The additional normal force exerted by an interfacial water molecule, i.e., the water-induced force, is calculated independently by inserting one single water molecule to 10 different interfacial positions and averaging the change in the normal force upon water molecule insertions. This procedure is repeated at each indentation depth. This step is important because the water molecule produced by the condensation reaction may diffuse around the interface, which results in the variation of the water-induced force. Our simulations show that the water-induced force does not show a trend with the indentation depth (see Fig. S1 in Supporting Information). Therefore, the water-induced force is averaged over different indentation depths in advance, and then added back to the calculation of bond-induced force at each indentation depth.

Here, we plot the water-induced force and the potential energy of one interfacial water molecule as a function of indentation depth. In the main text, we use the mean value of the water-induced force averaged over different indentation depths for the calculations of the bond-induced force of mechanism 1. The potential energy of water molecule is fitted with a linear function, which monotonically increases as a function of indentation depth. The fitted linear function is used for the calculation of the reaction energy of bonding mechanism 1 in section S5 below.

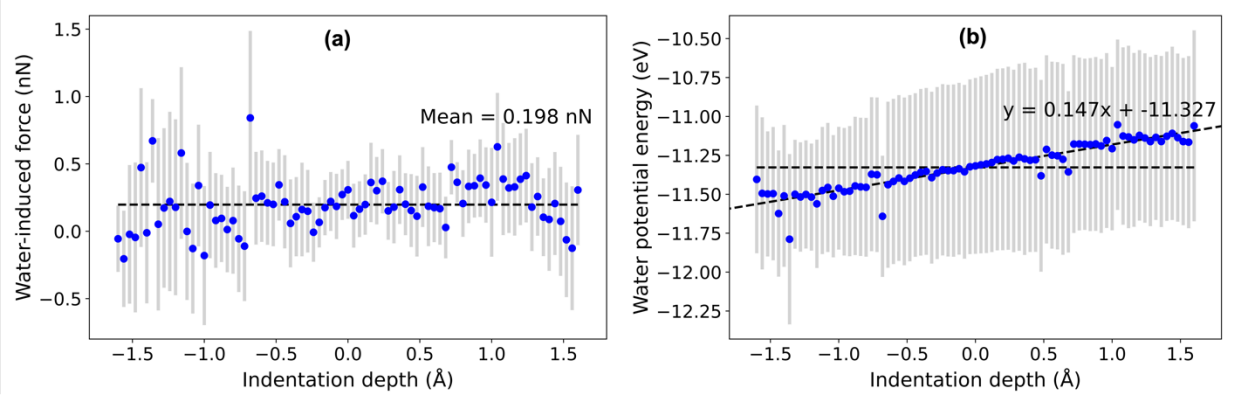


*Figure S1 (a) Water-induced force, i.e., the additional force exerted by the water molecule produced during the siloxane bonding reaction of mechanism 1, as a function of indentation depth. At each indentation depth, the water-induced force is averaged over 10 different interfacial water molecule positions. The grey line is the standard deviation, and the dashed line shows the mean value over different indentation depths. (b) The potential energy of interfacial water molecule as a function of indentation depth. At each indentation depth, the potential energy is averaged over 10 different interfacial water molecule positions. The horizontal dashed line shows the mean value over different indentation depths. The tilted dashed line is the linear fitting to the blue data points, where the fitted equation is shown on the plot. For both (a) and (b), 0 Å indentation depth is defined as in the main text.*

## S3 Bond-induced force from multi-bond interfaces

In the main text, we sampled the bond-induced force at different indentation depths by manually forming the single interfacial bond at different position across the interface. Instead, the bond-induced force can also be calculated from the interfaces with multiple interfacial bonds. The bond-induced force calculated with the data of multi-bond interfaces can be used to examine

whether neighbor interactions between already formed bonds impact the energy barriers for bond formation, as suggested before[7].

Here we take multi-bond interfaces where all the bonds are formed by mechanism 1 as an example. In Fig. S2 (a) we plotted the contact pressure as a function of the bond density (i.e., the number of bonds divided by the slab's nominal surface area) for different indentation depths. We define the interface without any manually-formed bonds as 0-bond interface. Those interfaces with different number of bonds are referred to as X-bond interface, where X represents the number of manually-formed bonds across the interface. The contact pressures of different 0-bond interfaces (the upper slab is shifted horizontally from the lower slab as explained in the main text) are different even at the same indentation depth. Since we only need to focus on the slope of the linear fitting, which is the bond-induced force, we shifted all the data points vertically, such that 0-bond interfaces have a pressure of 0 GPa for all interfaces and all indentation depths, and other (1-, 2-, 3-, 4-bond) interfaces are also shifted according to the corresponding 0-bond interface. The data points shown on the plot are averaged over different siloxane bond positions across all the interfaces at a given bond density and indentation depth. The error bars are the standard error of the means. The dashed lines are the linear fitting to the data at each indentation depth, whose slopes are the bond-induced force.

The bond-induced forces calculated from the multi-bond interfaces as a function of indentation depth are shown in Fig. S2 (b), where the horizontal line is the average over all indentation depths. The average bond-induced force obtained by this method is -0.47 nN, which differs only ~ 0.1 nN from the method with only one bond per interface considered (see the main text). The increasing trend shown in Fig. S2 (b) is also similar to the result shown in the main text. In other words, the effect of the neighbor interactions on bond-induced force is limited and therefore will be ignored in the main text.

Due to the limited instances of reactions by mechanism 2, no such calculations from multi-bond interfaces have been performed, but similar effect of the neighboring bonds could be expected.

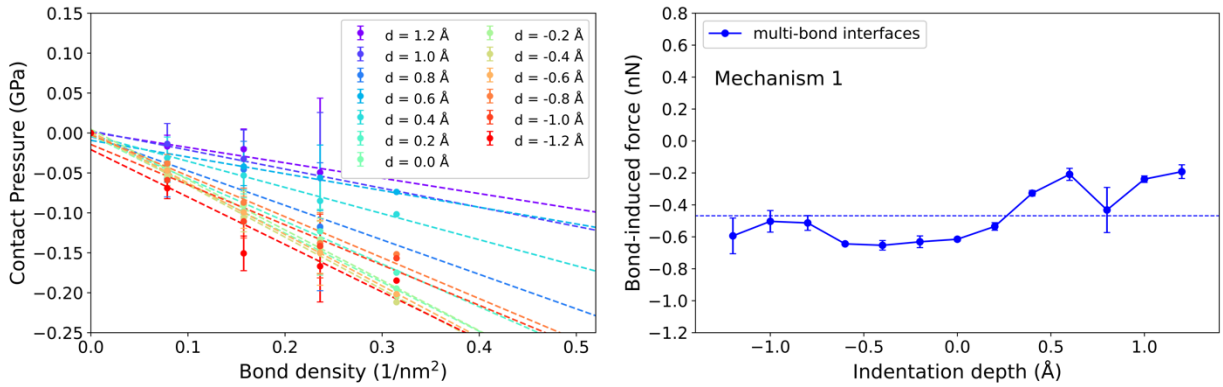


*Figure S2 (a) Contact pressures of silica slab-slab interface as a function of bond density at different indentation depths. The error bars are the standard error of means among different siloxane bond positions across the different slab-slab interfaces (*the upper slab is shifted horizontally from the lower slab*). The dashed lines are the linear fitting to the data at each indentation depths. (b) Bond-induced force as a function of the indentation depth. The error bars are the standard error of the fitted slopes in (a).*

## S4. Tip-substrate contacts and the contact mechanics

In the main text, we calculated the bond-induced force by conducting MD simulations on the flat interfaces. In order to further demonstrate that such bond-induced force also exists in the round tip-flat substrate contacts, such as those encountered in typical single-asperity AFM experiments, we created an amorphous silica tip with a spherical shape with a radius of ~9 nm. We then indented this large tip into the opposing silica substrate, up to the contact load of ~ 200 nN. The simulation result shows that there is a power-law area-load relationship as shown in Fig. S3 below, as expected for a typical contact mechanics model [10]. We then calculated the change in the contact load of the tip-substrate interface that results from forming interfacial bonds. The simulations of bonded interface are carried out at the highest indentation depth, and therefore highest contact load, of tip-substrate contacts during the indentation. The simulations for the reactions via mechanisms 1 and 2 are performed separately. The average bond-induced force is then obtained by dividing the change in the contact load by the number of interfacial bonds.

In order to show that our tip-substrate system is large enough for such calculation, Fig. S4 shows the strain distribution of the relaxed system with all the siloxane bonds of mechanism 1 considered for the bond-induced force calculation are formed. As it can be seen, the strain is localized at the near-surface contact region, and therefore, the effect of system-size on the bond-induced force in our MD simulations should be negligible. Therefore, the bond-induced force obtained from our MD simulations should be transferable to even larger contact sizes.

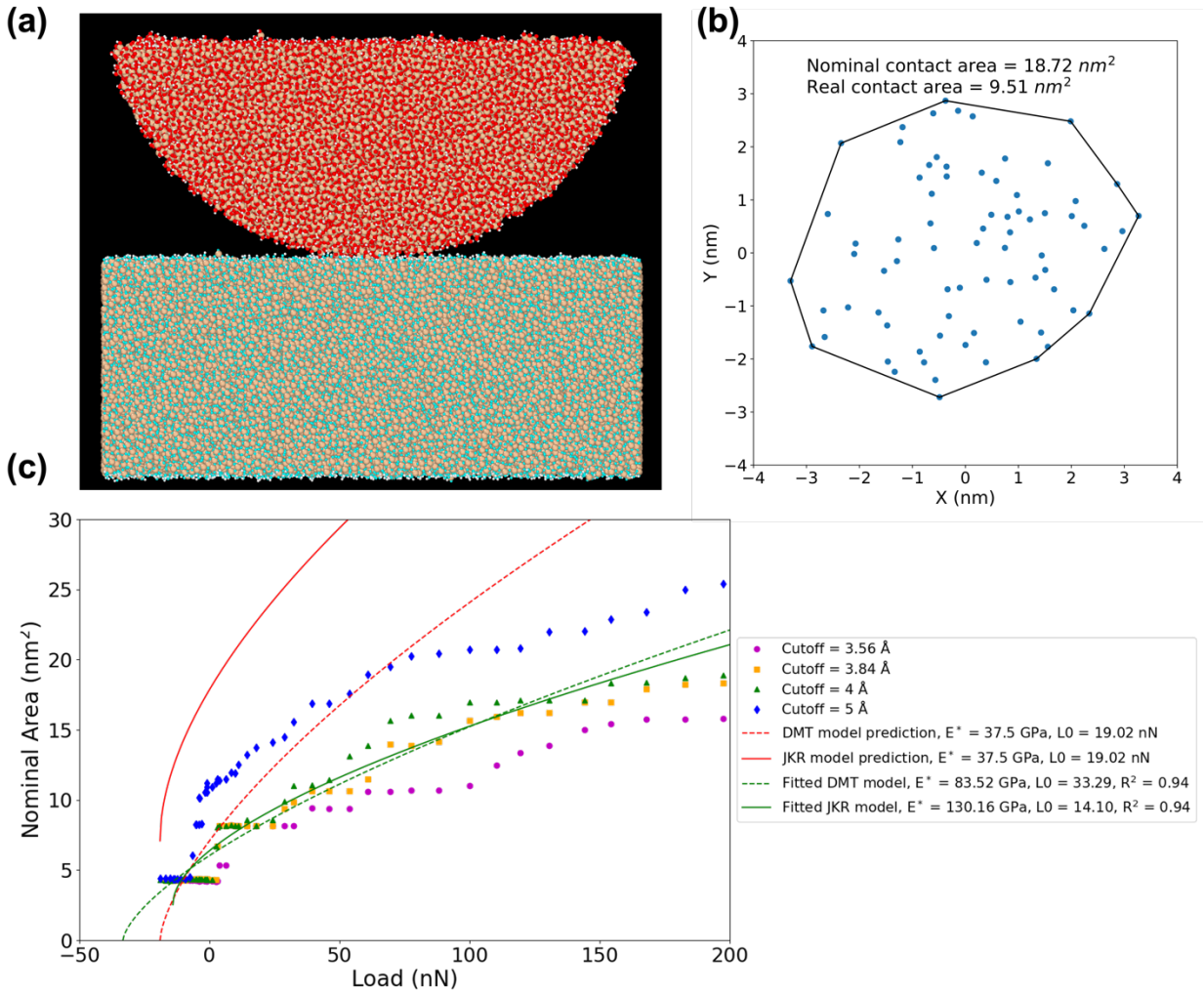


*Figure S3 (a) A snapshot from MD simulations of an amorphous silica tip with radius of curvature of 9 nm on top of an amorphous silica substrate. The red, cyan, beige, and white colors represent, O in the tip, O in the substrate, Si, and H, respectively. (b) The nominal contact area at a given contact load is obtained by the convex hull of the contacting Si-Si pairs with a given cutoff distance*[11]*. The real contact area is the product of the number of contacting Si-Si pairs and the area per Si atom. Here, the cutoff distance is 4 Å, the area per Si is 0.127 $nm^2$, and the contact load is 197.4 nN. The area per Si is determined by the square of the cube root of the silica density of 2.2 $g/cm^3$* [3]*. (c) The nominal contact area between the tip and the substrate as a function of the applied load with different Si-Si cutoff distances. Here, the nominal area is an average of areas determined from the convex hull on the tip's surface and on the substrate's surface. The red curves are the DMT (dashed) and JKR (solid) model predictions with the experimentally obtained effective Young's modulus*[8]*, and the pull-off force $L_0$ (the largest adhesion force during pulling off the tip) obtained by our MD simulations where the tip is pulled off from the substrate. Green curves are obtained by fitting with DMT and JKR models to the MD simulation results with cutoff distance of 4 Å, where the Young's modulus and the pull-off are set as free parameters. Both types of fits (green curves) result in the error $R^2$ of 0.94.*

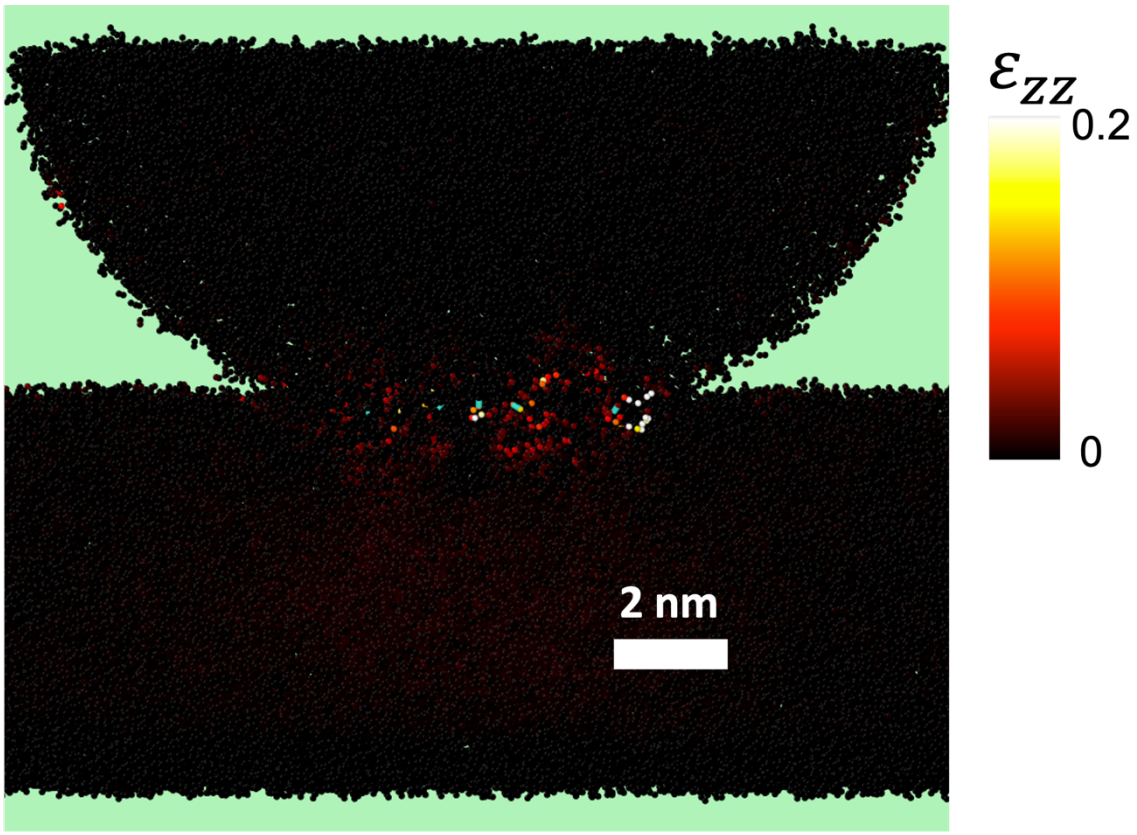


*Figure S4, Strain distribution at the bonded interface. Here, the zz component of the local strain tensor is calculated with the atomic strain algorithm implemented in OVITO*[4]*, where the cutoff radius of local spherical volume surrounding each atom for computing the strain tensor is set as 4 Å. The interfacial bonds, i.e., $Si_{up}$-$O_{low}$ or $Si_{low}$-$O_{up}$, are colored cyan. Here, the* subscripts $_{up}$ and $_{low}$ represent atoms in the upper and lower silica slabs, respectively.

## S5. Reaction energy of interfacial siloxane bonding

Here, the reaction energy of siloxane bonding, i.e., the energy difference between 0- and 1-bond interface of different mechanisms are plotted as a function of indentation depth as shown in Figs. S5 (a) and S5 (b). For mechanism 1, we use two different ways to calculate the reaction energy, which is the same as the two methods mentioned for the bond-induced force in the main text and section S3. The reaction energies of multi-bond interfaces at different indentation depths for the reaction mechanism 1 are obtained from the slopes of the linear fitting shown in Fig. S5 (c). In Fig. S4 (c), the potential energy is plotted as a function of the bond density. The data points are averaged following the same procedure that is used for the bond-induced force as explained in the section S3.

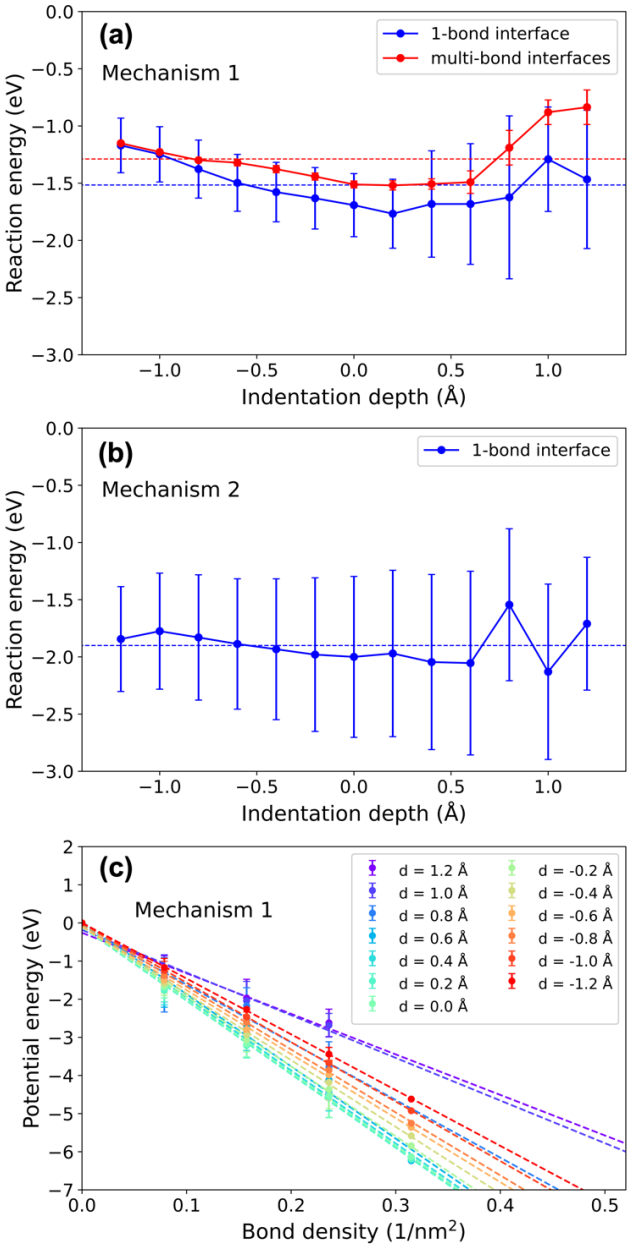


*Figure S5 (a) and (b) Reaction energy as a function of indentation depth for different bonding mechanisms. (a) Results for mechanism 1. Blue data is sampled from 1-bond interfaces (only 1 manually formed bonds), and red data is sampled from 1-, 2-, 3-, and 4-bond interfaces. The error bars on the blue points are standard error of means, and the error bars for the red points are the standard error of the fitting slopes. (b) Results for mechanism 2 at 1-bond interfaces. The error bars on the blue points are standard error of means. The dashed horizontal lines in (a) and (b) is the mean values of bond-induced force averaged over different indentation depths. (c) Potential energy of silica slab-slab interface as a function of bond density at different indentation depths for the reaction mechanism 1. The error bars are the standard error of means among different siloxane bond positions across the different slab-slab interfaces (*the upper slab is shifted horizontally from the lower slab*). The dashed lines are the linear fitting to the data at each indentation depths.*

## S6. Mechanochemical effect in chemical creep

Another interesting observation from Fig. 4 in the main text is that the effect of chemical creep on the increase in the number of bonds is slightly more significant than on the nominal contact area. Here, the amount of the effect of chemical creep is quantified by the percentage increase in the number of bonds $N$ and the nominal contact area $A$ relative to the values without creep, which are $N_0$ and $A_0$, respectively. The values of the percentage increases at selected times are listed in Table S1 and Table S2, for exothermic and endothermic interfaces, respectively. The time evolution of $N/N_0$ and $A/A_0$, as a function of contact time are shown in Fig. S6.

For exothermic interface, the larger increase in the number of bonds than in the nominal contact area can be observed for both cases of $\langle F_{bond} \rangle = -0.2$ nN and $\langle F_{bond} \rangle = -0.4$ nN. For instance, at $10^4$ s and with $\langle F_{bond} \rangle = -0.2$ nN on exothermic interface, the percentage increase in the number of bonds is 28 % relative to the values for the interface without creep, but it is only 23 % for the nominal contact area. A similar trend can be observed for the case of $\langle F_{bond} \rangle = -0.4$ nN on the exothermic interface, e.g., at $10^4$ s, there is a 64 % increase in the number of bonds and a 56 % increase in the nominal contact area, both relative to the values of the interface without creep.

This trend can be attributed to the mechanochemical effect included in our kMC model model[5], i.e., the pressure-dependent energy barriers as described by Eyring model[6]. With such mechanochemical effect, the increase in the nominal contact area not only provides a greater number of available reactions sites, but also accelerates the bonding reactions across the interface. Specifically, in our model the energy barriers at each reaction site are modified by the local contact pressure, i.e., $E_{b,form} = E_{b,form,0} - \Delta V_{form} P_{local}$ and $E_{b,break} = E_{b,break,0} - \Delta V_{break} P_{local}$. Here, $E_{b,form,0}$ and $E_{b,break,0}$, respectively, are the energy barriers for bond formation and breaking at zero pressure, $\Delta V_{form}$ and $\Delta V_{break}$ are the activation volumes for the bond formation and breaking, respectively, and $P_{local}$ is the local contact pressure, which is obtained from the DMT model[12].

Due to the 2/3 power-law dependence of the nominal contact area on the total normal load in the DMT model, the average contact pressure $P_{average}$ is proportional to $\sqrt{A}$, where $A$ is the nominal contact area. The local contact pressure $P_{local}$ at a given radial distance from the center of the contact in DMT scales linearly with $P_{average}$, and therefore, $P_{local} \sim \sqrt{A}$. This indicates that the local pressures across the interface of a single asperity contact continuously increase as the nominal contact area increases due to the chemical creep.

In our model, we assume that $\Delta V_{form}$ is positive, based on previous theoretical studies[7,13] on pressure effects on siloxane bond formation. We also assume a negative value for $\Delta V_{break}$ based on Bronsted–Evans–Polanyi relation[14], where the change in the energy barrier for forward and backward reactions is of the opposite sign. As a result, the compressive local pressure will result in a reduction of $E_{b,form}$, and in an increase of $E_{b,break}$. In other words, the interface becomes more and more prone to bonding with a faster reaction rate of bond formation as the area and the pressure increase. As a result, the number of bonds increases faster than the nominal contact area due to the coupling of the chemical creep and the mechanochemical effect. For comparison, we have also performed kMC simulations with the same parameters, but without the mechanochemical effect included (i.e., $\Delta V_{form} = \Delta V_{break} = 0$ Å$^3$). The simulation results are shown in Fig. S7 and listed in Table S3. We found that in such case, the difference between the rates of change of the number of bonds and of the nominal contact area is smaller than in simulations with the mechanochemical effect included.

The values for the endothermic interface with non-zero activation volumes are shown in Table S2. Unlike the exothermic interface, the mechanochemical effect on the endothermic interfaces is only apparent for the case of $\langle F_{bond} \rangle = -0.4$ nN. For example, at contact time of $10^4$ s, the percentage increase in the number of bonds is 23 %, and the percentage increase in the nominal contact area is only 17 %. However, such mechanochemical effect cannot be observed for the case with $\langle F_{bond} \rangle = -0.2$ nN. For instance, at the time of $10^3$ s both the number of bonds and the nominal contact area increases by 8 % compared to the case without creep. At $10^4$ s, the predicted 6 % increase in the number of bonds is even smaller than the predicted 8 % increase in the contact area, although such difference is within the error bars as shown in Fig. S6. The negligible mechanochemical effect is due to the less significant chemical creep for the endothermic interface with less adhesive bonds, where neither the contact area nor local contact pressures increases significantly as a function of the contact time.

It is interesting to compare our results to our previously reported kMC simulations on randomly rough elastic contacts[15], where no creep was considered. In that study, we found that the mechanochemical effect will lead to lower reaction energy barriers at those asperities that have high local contact pressures within the rough contact. Specifically, the local pressures are pre-determined by numerical contact mechanics model for the elastic rough contacts before the ageing starts, and those reaction sites under high compressive stress will have fast reaction rates due to the mechanochemical coupling. As a result, those highly reactive sites will be consumed for bond formation at relatively short time scale (< 10 s). The mechanochemical effect becomes less important at longer time scale, where only reactions sites with lower local pressures are available for bonding. In contrast, our current study indicates that the mechanochemical effect becomes more and more important as ageing goes on at single-asperity level due to the chemical creep.

*Table S1: Percentage increase in the number of bonds $N$ and the nominal contact area $A$ for exothermic interface relative to the values without creep, which are $N_0$ and $A_0$, respectively.*

| Contact time (s) | | 10 | $10^2$ | $10^3$ | $10^4$ |
|---|---|---|---|---|---|
| $\langle F_{bond} \rangle = -0.2$ nN | $N/N_0$ | 9 % | 15 % | 21 % | 28 % |
| | $A/A_0$ | 8 % | 13 % | 18 % | 23 % |
| $\langle F_{bond} \rangle = -0.4$ nN | $N/N_0$ | 18 % | 26 % | 44 % | 64 % |
| | $A/A_0$ | 16 % | 27 % | 40 % | 56 % |

*Table S2: Percentage increase in the number of bonds $N$ and the nominal contact area $A$ for an endothermic interface relative to the values without creep, which are $N_0$ and $A_0$, respectively.*

| Contact time (s) | | 10 | $10^2$ | $10^3$ | $10^4$ |
|---|---|---|---|---|---|
| $\langle F_{bond} \rangle = -0.2$ nN | $N/N_0$ | 3 % | 11 % | 8 % | 6 % |
| | $A/A_0$ | 5 % | 7 % | 8 % | 8 % |
| $\langle F_{bond} \rangle = -0.4$ nN | $N/N_0$ | 10 % | 23 % | 24 % | 23 % |
| | $A/A_0$ | 10 % | 14 % | 16 % | 17 % |

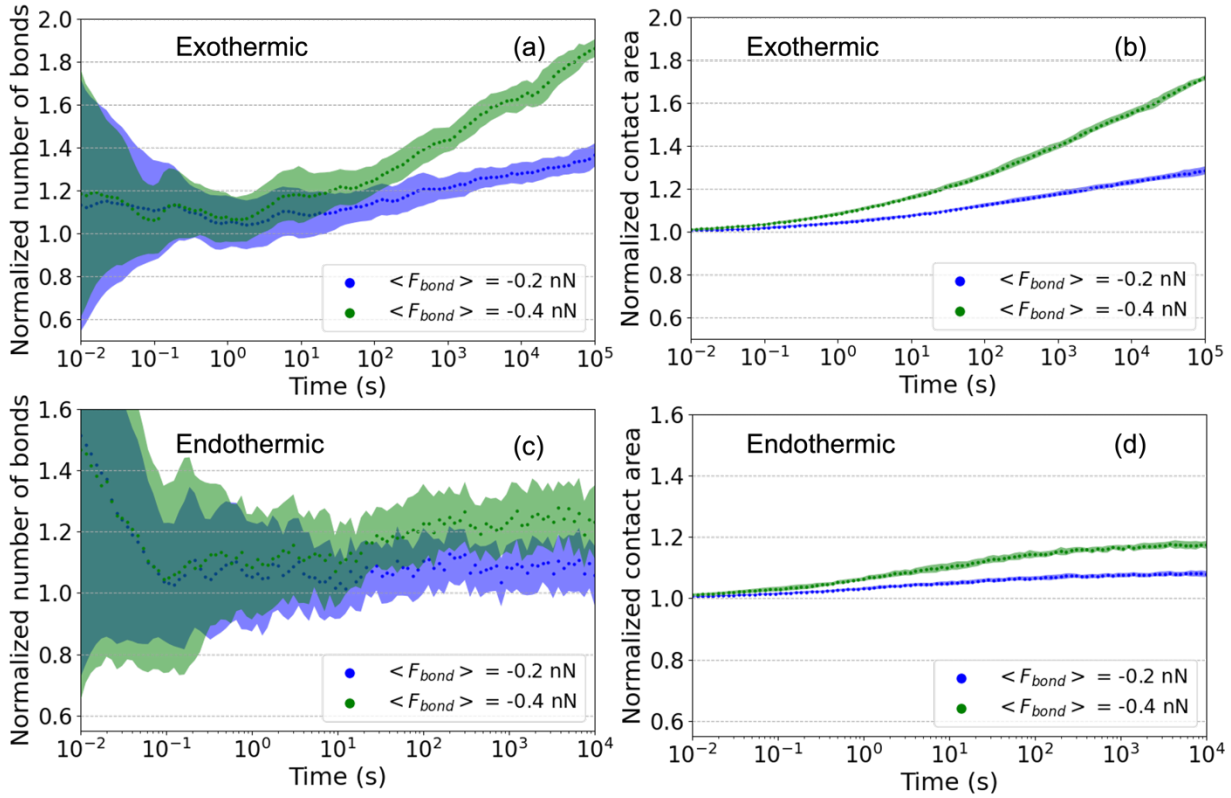


*Figure S6 Results of kMC simulations of time evolution of the number of bonds and the nominal contact area normalized by the values for the interfaces without the creep. Results for [(a) and (b)] exothermic interface, and [(c) and (d)] endothermic interface with different distributions of bond-induced force* $F_{bond}$

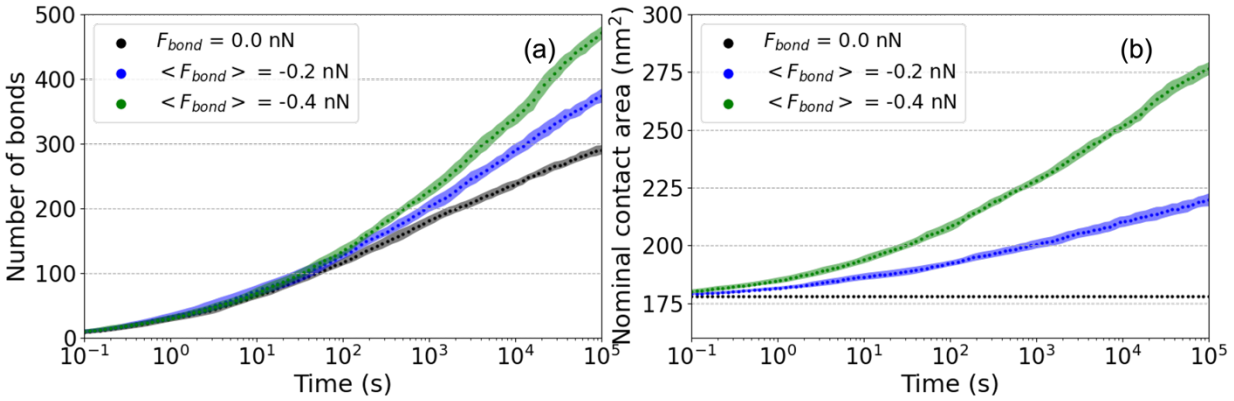


*Figure S7 kMC simulation results for exothermic interface without the mechanochemical effect. Time evolution of (c) the number of bonds and (d) the nominal contact area.*

*Table S3: Percentage increase in the number of bonds N and the nominal contact area A for exothermic interface relative to the values without creep, which are $N_0$ and $A_0$, respectively, without the mechanochemical effect.*

| Contact time (s) | | 10 | $10^2$ | $10^3$ | $10^4$ |
|---|---|---|---|---|---|
| $\langle F_{bond} \rangle = -0.2$ nN | $N/N_0$ | 12 % | 9 % | 12 % | 22 % |
| | $A/A_0$ | 5 % | 8 % | 13 % | 18 % |
| $\langle F_{bond} \rangle = -0.4$ nN | $N/N_0$ | 6 % | 15 % | 25 % | 44 % |
| | $A/A_0$ | 9 % | 17 % | 28 % | 42 % |

## References


(1) Yeon, J.; Van Duin, A. C. T. ReaxFF Molecular Dynamics Simulations of Hydroxylation Kinetics for Amorphous and Nano-Silica Structure, and Its Relations with Atomic Strain Energy. *J. Phys. Chem. C* **2015**, *120* (1), 305–317. https://doi.org/10.1021/acs.jpcc.5b09784.

(2) Plimpton, S. Fast Parallel Algorithms for Short-Range Molecular Dynamics,. *Journal of Computational Physics*. 1995, pp 1–19. https://doi.org/10.1039/c7sm02429k.

(3) Mozzi, R. L.; Warren, B. E. Structure of Vitreous Silica. *J. Appl. Crystallogr.* **1969**, *2*, 164. https://doi.org/10.1038/147642b0.

(4) Stukowski, A. Visualization and Analysis of Atomistic Simulation Data with OVITO–the Open Visualization Tool. *Model. Simul. Mater. Sci. Eng.* **2010**, *18*, 015012.

(5) Li, Z.; Szlufarska, I. Multiphysics Model of Chemical Aging in Frictional Contacts. *Phys. Rev. Mater.* **2018**, *2* (6), 063602. https://doi.org/10.1103/PhysRevMaterials.2.063602.

(6) Eyring, H. Viscosity, Plasticity, and Diffusion as Examples of Absolute Reaction Rates. *J. Chem. Phys.* **1936**, *4*.

(7) Liu, Y.; Szlufarska, I. Chemical Origins of Frictional Aging. *Phys. Rev. Lett.* **2012**, *109* (18), 186102. https://doi.org/10.1103/PhysRevLett.109.186102.

(8) Tian, K.; Gosvami, N. N.; Goldsby, D. L.; Liu, Y.; Szlufarska, I.; Carpick, R. W. Load and Time Dependence of Interfacial Chemical Bond-Induced Friction at the Nanoscale. *Phys. Rev. Lett.* **2017**, *118* (7), 076103. https://doi.org/10.1103/PhysRevLett.118.076103.

(9) Zhuravlev, L. T. The Surface Chemistry of Amorphous Silica. *Colloids Surfaces A Physicochem. Eng. Asp.* **2000**, *173*, 1–38. https://doi.org/10.1016/S0927-7757(00)00556-2.

(10) Carpick, R. W.; Ogletree, D. F.; Salmeron, M. A General Equation for Fitting Contact Area and Friction vs Load Measurements Robert. *J. Colloid Interface Sci.* **1999**, *211* (2), 395–400.

(11) Mo, Y.; Turner, K. T.; Szlufarska, I. Friction Laws at the Nanoscale. *Nature* **2009**, *457* (7233), 1116–1119. https://doi.org/10.1038/nature07748.

(12) Derjaguin, B. V; Muller, V. M.; Toporov, Y. P. Effect of Contact Deformations on the Adhesion of Particles. *J. Colloid Interface Sci.* **1975**, *53* (2), 314–326.

(13) Li, Z.; Szlufarska, I. Physical Origin of the Mechanochemical Coupling at Interfaces. *Phys. Rev. Lett.* **2021**, *126* (7), 76001. https://doi.org/10.1103/PhysRevLett.126.076001.

(14) Evans, M. G.; Polanyi, M. Inertia and Driving Force of Chemical. *Trans. Faraday Soc.* **1938**, *34*, 11–24.
(15) Li, Z.; Pastewka, L.; Szlufarska, I. Chemical Aging of Large-Scale Randomly Rough Frictional Contacts. *Phys. Rev. E* **2018**, *98* (2), 023001. https://doi.org/10.1103/PhysRevE.98.023001.